A Model for Ionic Conduction in the Ryanodine Receptor Channel of Sheep Cardiac Muscle Sarcoplasmic Reticulum

Andrew Tinker, Allan R. G. Lindsay, and Alan J. Williams

From the Department of Cardiac Medicine, National Heart and Lung Institute, University of London, London SW3 6LY, United Kingdom

ABSTRACT A model is developed for ionic conduction in the sheep cardiac sarcoplasmic reticulum ryanodine receptor channel based on Eyring rate theory. A simple scheme is proposed founded on single-ion occupancy and an energy profile with four barriers and three binding sites. The model is able to quantitatively predict a large number of conduction properties of the purified and native receptor with monovalent and divalent cations as permeant species. It suggests that discrimination between divalent and monovalent cations is due to a high affinity central binding site and a process that favors the passage of divalent cations between binding sites. Furthermore, differences in conductance among the group Ia cations and among the alkaline earths are largely explained by differing affinity at this putative central binding site.

INTRODUCTION

One of the earliest attempts to describe ionic electrodiffusion in biological membranes was made by Goldman (1943) and is known as constant field theory. It was subsequently adapted by Hodgkin and Katz (1949). In their description, ionic flux and thus current is dependent on ionic concentration on either side of the membrane, applied voltage, and a permeability coefficient unique for the specified ion in the membrane. There is a single measure of ionic selectivity. An important assumption in such schemes is that each ion moves independently of other ions in the system. As was argued in the preceding paper (Tinker and Williams, 1992) and in previous work from this laboratory (Lindsay, Manning, and Williams, 1991), this is clearly not the case in the sheep cardiac sarcoplasmic reticulum (SR) ryanodine receptor channel.

Similar divergence from independence in other biological channels has led to the development of other approaches. The most successful of these has been the use of Eyring rate theory. This represents ionic movement through channel proteins as a series of jumps between binding sites, equivalent to energy minima or "wells," over energy maxima or "peaks." The energy profile is assumed to be static and fixed,

though treatments are available that take fluctuations, occurring either spontaneously or on ion binding, into account (Lauger, Stephan, and Frehland, 1980).

The predictions from such models are dependent on the type of coupling between the ions. Ions may be uncoupled in their movement but would then obey the independence relation; such a system does not adequately explain ionic conduction in the ryanodine receptor channel. Alternatively, ions may move in single-file with either single or multiple occupancy of the channel conduction pathway. The purified sheep cardiac SR ryanodine receptor channel as detailed in our previous work displays many properties consistent with single-ion occupancy (Lindsay et al., 1991; Tinker and Williams, 1992). To further elucidate the mechanisms underlying ionic selectivity, we have attempted to model ion conduction in the sheep cardiac SR Ca^{2+} release channel/ryanodine receptor channel using Eyring rate theory. In addition, we present further experimental evidence on the interaction of Cs^+, $Tris^+$, and the divalent cations with the conduction pathway of the receptor channel.

METHODS

Purification of the Sheep Cardiac Ryanodine Receptor Channel

The experimental methods used were identical to those described in the preceding communication (Tinker and Williams, 1992) and they are not repeated here. The reader is referred to that paper for details.

Planar Lipid Bilayer Methods

The methods and experimental conditions were similar to those described in the preceding paper (Tinker and Williams, 1992). For the series of experiments described in which conductance was investigated using symmetrical Cs^+ solutions, the channels were incorporated in the relevant Cs^+ concentration, fusion being induced by the addition of K^+ to the cis chamber to form an osmotic gradient. After incorporation, the cis chamber was perfused with the desired Cs^+ concentration. Ion activities were obtained for the inorganic monovalent cations from Hamer and Wu (1972), for Ba^{2+}, Mg^{2+}, and Ca^{2+} from Scatchard and Theft (1930), both given in Lobo (1989), and for $Tris^+$ and Sr^{2+} from Kielland (1937), given in Kortum and Bockris (1951).

Single-Channel Data Acquisition and Analysis

Single-channel current fluctuations were analyzed as detailed in the preceding article (Tinker and Williams, 1992).

Theory

Eyring rate theory and its application to single-ion occupancy have been addressed by a number of authors and the results are well known (for details, see Lauger, 1973; Hille, 1975, 1984). The novelty of our approach is that a general solution of the state diagram is obtained and then translated to a computer algorithm within the body of a single program. The graphical method of King and Altman (1956) is used as the basis for this algorithm. The problem is solved for the general case for two ions which may be either mono- or divalent. Single-ion models possess the advantage that experimental observations can be interpreted with more crispness in terms of the energy profile than in multi-ion models. The binding affinity depends simply on the well depth, and permeability ratios between ions depend simply

on differences in peak height. Ionic conductance is a complex function of the energy profile as a whole. A specific model is proposed and its application is illustrated in Results. Energy profiles are expressed in multiples of RT (R = gas constant, T = absolute temperature).

Details of the Computer Program

The algorithm was incorporated into a computer program written in basic 23 and run on a PDP 11/73 lab computer (Indec Systems, Inc., Sunnyvale, CA). The program forms the terms of the solution for the n barrier model to be tested. A variety of menus allow the details of the energy profiles and activities for the two ions to be entered. Treatment options are available for monovalent and divalent ions and for interactions between them.

The basic output is a current–voltage relationship that can be plotted if required. In mixed ionic conditions an option is available to calculate the reversal potential by a simple iterative routine. To measure ionic affinity the K_D was calculated at 50 mV (K_{D50}) in symmetrical ionic conditions by an iterative method based on half-saturating current. The K_{D50} was a very good approximation to the K_D determined experimentally from the conductance–activity relationship. In addition, the program provides the probability of a single channel being in a given kinetic state at 0 mV (or the fraction in a given kinetic state within a population of channels). In the text this figure is expressed as a percentage. A number of models were tried with a variety of energy profiles and barrier numbers. A fit was determined by trial and error.

A PC-executable version of the program is available to interested readers, together with brief details of the theory and the general solution of the state diagram. For a copy, please send a preformatted disk (either 5.25 or 3.5 inches) to the authors.

RESULTS

Considerations Concerning a Specific Model

Before detailing the application of the model and the new experimental observations, it is pertinent to review some features of ionic conduction in the sheep cardiac SR ryanodine receptor channel and consider how these have influenced the development of the model.

The current–voltage relationship is linear and symmetrical under symmetrical ionic conditions with monovalent cations as the permeant ion (Lindsay et al., 1991). The current–voltage relationships under symmetrical ionic conditions with the divalent cations as the permeant species are also symmetrical but show a small deviation from ohmic behavior at high holding potentials (see Tinker and Williams, 1992). The lack of rectification implies that the energy profile must be symmetrical about a central axis or that any asymmetry must have consequences that are undetectable within our limits of experimental error. In addition, ohmic behavior with monovalent cations can only be approached in models with more than three barriers. We have proposed the existence of at least two binding sites within the conduction pathway on the basis of blocking experiments with a series of small tetraalkyl ammonium cations (Tinker, Lindsay, and Williams, 1992). The effective valencies of block give sites located at ~50 and 90% of the way across the voltage drop from the cytosolic face of the channel protein and considerations of symmetry in the energy profile imply a further site located 10% of the voltage drop from this face. A 4-barrier model with binding sites at those locations was thus regarded as the necessary minimum.

In the forthcoming sections attempts are made to justify such a 4-barrier model.

Peak 1   Peak 2   Peak 3   Peak 4

0   0

Well 1   Central Well   Well 3

0   0.1   0.5   0.9   1
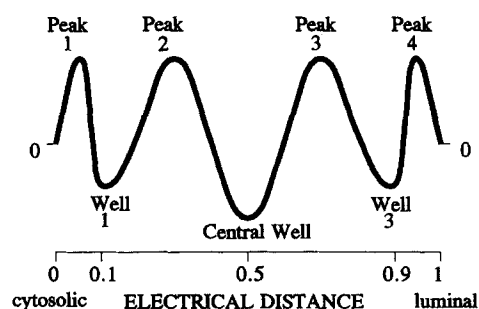cytosolic   ELECTRICAL DISTANCE   luminal

FIGURE 1. The specific voltage- and concentration-independent 4-barrier energy profile used to model ion translocation in the ryanodine receptor channel.

The specific voltage- and concentration-independent energy profile examined is illustrated in Fig. 1. The two binding sites on either side of the central well are assumed to be fixed in depth and to show little discrimination between permeant inorganic ions. Permeability differences for Cs^+ and alkaline earth divalent cations, relative to K^+, are explained by assumption of the peak offset condition; i.e., that the peak heights for a given ion vary by a fixed amount over each barrier when compared with that of another ion.

The ionic conduction of the organic cation $Tris^+$ is accounted for in a different way. It is assumed that $Tris^+$ interacts with equal affinity at all three sites. This is not an unreasonable proposal, as we have suggested that the TEA^+ binding site is hydrophobic in nature and as a result the large organic cation $Tris^+$ would be expected to bind with higher affinity to this site when compared with inorganic monovalent and divalent cations. To explain all the experimental data for $Tris^+$, permeability differences are accounted for by a change in peak height over one particular barrier, i.e., a selectivity filter. Again this seems reasonable, as this may correspond to the point of maximal narrowing of the pore. The parameters used for all modeled ions are shown in Tables I and II.

Current–Voltage Relationships in Symmetrical 210 mM Salt

The model accurately predicts the single-channel current–voltage relationships in symmetrical 210 mM monovalent cation. In symmetrical 210 mM divalent cation the model follows the experimental points between ±60 mV holding potential but deviates increasingly from the data as the holding potential becomes increasingly positive or negative. This discrepancy is explored further below. Figs. 2 and 10 *A*

TABLE I

Parameters Used for the Voltage- and Concentration-independent Energy Profiles for the Monovalent Cations

Ion	Peak 1	Peak 2	Peak 3	Peak 4	Well 1	Central well	Well 3
				RT			
Cs^+	6.15	6.15	6.15	6.15	−2.35	−2.35	−2.35
K^+	5.50	5.50	5.50	5.50	−2.35	−3.25	−2.35
Na^+	5.50	5.50	5.50	5.50	−2.35	−4.00	−2.35
Li^+	5.50	5.50	5.50	5.50	−2.35	−5.00	−2.35
$Tris^+$	5.50	5.50	9.40	5.50	−3.75	−3.75	−3.75

TABLE II

Parameters Used for the Voltage- and Concentration-independent Energy Profiles for the Divalent Cations

Ion	Peak 1	Peak 2	Peak 3	Peak 4	Well 1	Central well	Well 3
				RT			
Ca^{2+}	3.00	3.00	3.00	3.00	−2.35	−9.50	−2.35
Ba^{2+}	3.25	3.25	3.25	3.25	−2.35	−9.15	−2.35
Sr^{2+}	3.00	3.00	3.00	3.00	−2.35	−9.45	−2.35
$Mg^{2+}.1$	3.00	3.00	3.00	3.00	−2.35	−9.80	−2.35
$Mg^{2+}.2$	3.30	3.30	3.30	3.30	−2.35	−9.50	−2.35

illustrate the fit of the model to the experimentally determined points with K^+ and Ba^{2+} as examples.

Saturation of Single-Channel Conductance in Monovalent Cations

The dependence of single-channel conductance on the surrounding ion activity was determined for Cs^+. In a fashion similar to the other monovalent cations (K^+, Na^+, and Li^+) (Lindsay et al., 1991), conductance reached a plateau as ion activity increased. The resulting conductance–activity relationship on the basis of conductance measurements (the mean of $n = 4$ bilayers) at five separate activities could be described by Michaelis-Menten–type kinetics and by using nonlinear regression (Enzfitter; Biosoft, Cambridge, UK), a K_D and G_{max} of 34 mM and 588 pS were estimated for Cs^+ (data not shown). Measurements at and below 50 mM Cs^+ were not possible because of a marked decline in single-channel P_o at ionic concentrations
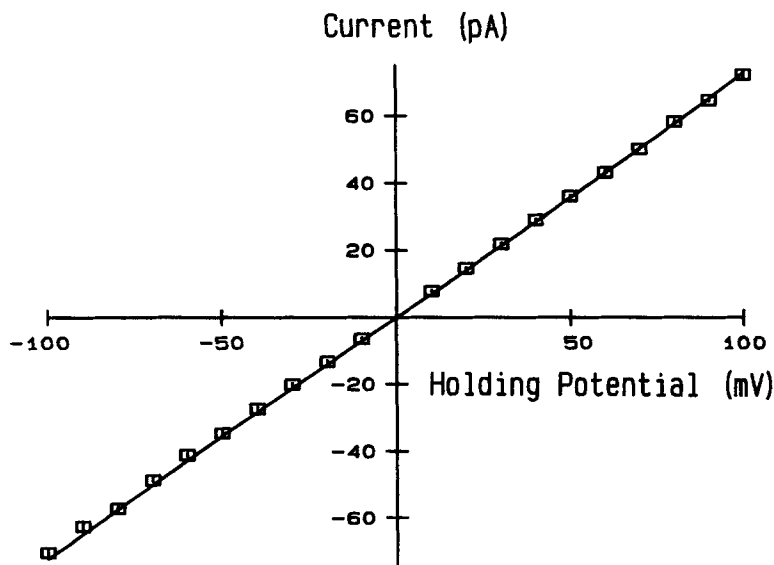

FIGURE 2. The single-channel current–voltage relationship in symmetrical 210 mM K^+. The experimental points ($n = 6$, ±SEM) are indicated by the squares, and the solid line is the model prediction from the energy profile given in Table I.

below this level. Under these conditions P_o was unresponsive both to Ca^{2+} and to secondary agonists such as caffeine. In view of the difficulty of obtaining points below the K_D, the value quoted ought to be viewed as an upper estimate.

Comparisons of the model predictions for K_D and G_{max} with the experimentally determined best fit parameters for a range of monovalent cations are shown in Table III. The model fit was obtained by performing a computer simulation of the relevant experiments and using nonlinear regression (Enzfitter; Biosoft) to obtain the best rectangular hyperbola that described the data generated by the model. In addition, the predicted single-channel conductance in symmetrical 210 mM salt is compared with the experimentally observed value. From Table III it is apparent that the model and observed conduction parameters vary as a rule by <15% for the group Ia cations.

TABLE III

Comparison of the Observed and Predicted Conduction Parameters for the Monovalent Cations

Ion	K_D Observed/predicted	G_{max} Observed/predicted	G_{210} Observed/predicted	P_{X^+}/P_{K^+} Observed/predicted
	mM	*pS*	*pS*	
Cs^+	34/34	588/621	460/500	0.61/0.50
K^+	20/23	900/831	723/712	1.00/1.00
Na^+	18/15	516/530	446/481	1.15/1.02
Li^+	9.1/7.4	248/244	215/234	0.99/1.05
$Tris^+$	—/5.4	—/25	17/24	0.22/0.20

G_{210} is the conductance in 210 mM symmetrical salt and P_{X^+}/P_{K^+} is the permeability ratio relative to K^+. K_D and G_{max} are as defined in the text. Observed conduction parameters from Lindsay et al. (1991) and this paper.

The Interaction of Monovalent Cations

There is little or no permeability difference between Na^+, K^+, and Li^+ (Lindsay et al., 1991). The difference seen experimentally in conductance between these ions can be solely accounted for in the model by changes in affinity at the central binding site (Table I). The situation with Cs^+ is different as it is significantly less permeant than K^+ in the receptor channel (P_{Cs^+}/P_{K^+} = 0.61; Lindsay et al., 1991). This permeability difference is modeled by the peak offset condition. Despite this added complexity, the predicted conductance with symmetrical 210 mM Cs^+, the K_D and G_{max} are close to experimental values (Table III). The small differences apparent in the predicted permeability ratios for Na^+, K^+, and Li^+ in Table III arise because of the small differences in activity at equivalent ionic concentrations.

In addition, the model can forecast the interaction between monovalent cations. For example, it predicts the behavior of single-channel current under bi-ionic conditions. This is illustrated for Li^+ and K^+ in Fig. 3. It also describes the behavior of single-channel conductance with varying Li^+-K^+ and Na^+-K^+ mole fraction (data not shown).

A Model for Tris⁺

The large organic cation Tris⁺ is able to act as a current carrier in the ryanodine receptor channel, but displays low conductance and permeability when compared with K⁺. A further independent test of any model derived from these data would be to predict the interaction of Tris⁺ and K⁺. Fig. 4 illustrates such experiments. The addition of 20 mM Tris⁺ to *cis* and *trans* chambers in the presence of 210 mM K⁺ results in a significant reduction in single-channel current amplitude when compared with control (cf. Figs. 2 and 4). The "block" is asymmetrical, being more prominent at positive holding potentials. The interpretation of permeant ion block is complex but is possible within the context of the model. The asymmetry of block is best
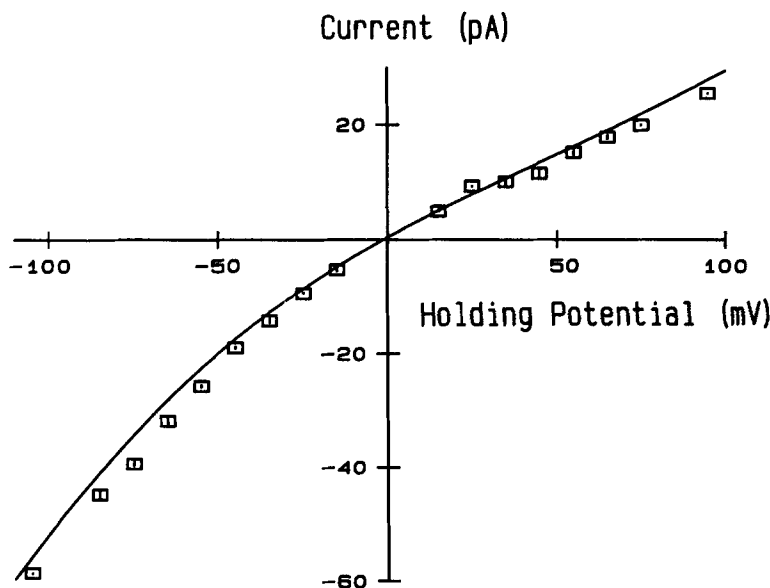

FIGURE 3.   The single-channel current–voltage relationship under bi-ionic conditions with 210 mM Li⁺ in the *cis* chamber and 210 mM K⁺ in the *trans* chamber. The experimental points are from Lindsay et al. (1991) and are indicated by squares ($n = 4$, ±SEM). The solid line is the fit generated by the model given in Table I.

modeled by assuming that peak 3 is much higher for Tris⁺ than K⁺. There are other ways to reproduce asymmetry, such as an inequality in binding between sites 1 and 3 or by assuming that selectivity occurs over peak 4. However, models based on these changes do not fit the experimental data as well. It is likely that the true situation is a complex combination of these various possibilities. Despite these reservations, the model reproduces closely the observed blocking behavior and the conduction and permeability characteristics of Tris⁺ (Fig. 4 and Table III).

The experimentally observed single-channel current–voltage relationship in symmetrical 210 mM Tris⁺ is symmetrical with a low conductance (see Table III and Lindsay et al., 1991). The predicted single-channel current–voltage relationship with

this model under the same ionic conditions shows some rectification. The magnitude of the effect, however, is small in absolute terms; for example, at a holding potential of 80 mV the predicted single-channel current is 2.07 pA and at −80 mV it is −1.73 pA. The difference of only 0.34 pA would be difficult to resolve experimentally.

Extending the Model to Divalent Cations

It is obviously important to try to extend this treatment to the physiological charge carrier Ca^{2+} and also to the other divalent cations. As detailed in Tinker and Williams (1992), the divalent cations are more permeable than monovalents in the sheep cardiac SR ryanodine receptor channel. The model assumes that there is no
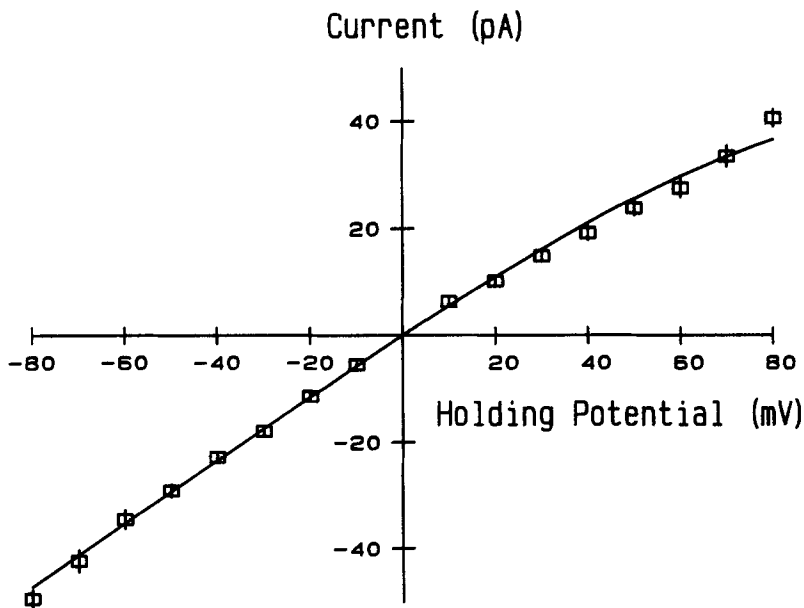

FIGURE 4. The current–voltage relationship in symmetrical 210 mM K^+ seen after the addition of 20 mM $Tris^+$ to the cis and trans chambers. The experimental points are indicated by squares ($n = 5$, ±SEM) and the line is the fit generated by the model given in Table I.

permeability difference between Ca^{2+}, Mg^{2+}, and Sr^{2+}, although Ba^{2+} is slightly less permeable than the other alkaline earths. Once again the permeability difference relative to K^+ is modeled using the peak offset condition. The energy profiles used for the divalent cations are shown in Table II. The predicted and observed conduction parameters, as far as they are known, are shown in Table IV. The small differences apparent in the modeled permeability of Ca^{2+}, Sr^{2+}, and Mg^{2+} relative to K^+ arise because of the small differences in activity of these cations at equivalent ionic concentrations.

Imposing the above limitation on the concentration- and voltage-independent energy profiles of the divalent cations means that to achieve currents with the model approaching those seen experimentally the K_D for the divalent cations must be in the

TABLE IV

Observed and Predicted Conduction Parameters for the Divalent Cations

Ion	Predicted K_m	Conductance Observed/predicted	$P_{X^{2+}}/P_{K^+}$ Observed/predicted
	mM	*pS*	
Ca^{2+}	0.116	94/94*	6.50/7.15
Ba^{2+}	0.165	199/191‡	5.80/5.28
Sr^{2+}	0.123	183/181‡	6.70/5.88
Mg^{2+}.1	0.086	—/128‡	5.90/6.93
Mg^{2+}.2	0.116	—/128‡	5.90/5.21

*The figure given is obtained for the receptor channel under those conditions used for the native channel (see text).

‡The figure given is obtained from the current–voltage relationship between 60 and −60 mV holding potential under symmetrical ionic conditions.

range of 100 μM. In the preceding study high single-channel conductance was found at very low symmetrical Ba^{2+} activities. Although the figure obtained for K_D was higher than predicted by the model, it was in the right range. In addition, there are reasons to view the observed K_D as an upper limit. Given this, are there any other means to examine the affinity of the conduction pathway for the divalent cations?

One possible method is to examine the influence of the divalent cations on K^+ current. In other words, do divalent cations block monovalent current? The addition of 1–10 mM divalent cation either to the *trans* chamber or symmetrically led to a significant reduction in single-channel K^+ current amplitude. Examples are shown in Fig. 5.

Two kinds of experiment were performed. In the first, the concentration dependence of the reduction in single-channel current amplitude was determined for Ba^{2+}. The experiments were performed in symmetrical 210 mM K^+ and control currents were initially obtained at holding potentials of ±60 mV. Increasing concentrations of Ba^{2+} were then aliquoted into both *cis* and *trans* chambers and the effect on the single-channel current–amplitude relationship was calculated at ±60 mV. In these
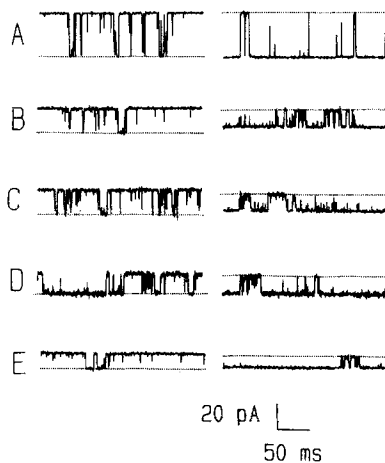

FIGURE 5. Representative single-channel current fluctuations at a holding potential ±50 mV. The left panel shows traces at 50 mV and the right at −50 mV. The dotted line indicates the current amplitude of a channel opening. The control traces in symmetrical 210 mM K^+ are shown in *A*, following the addition of 5 mM Ca^{2+} and Mg^{2+} to the *trans* chamber in *B* and *C*, respectively, and 10 mM Ba^{2+} and Ca^{2+} symmetrically in *D* and *E*, respectively.

experiments the single-channel current–amplitude relationship was reduced to a greater extent at -60 than at $+60$ mV. A similar asymmetry was observed in experiments performed with symmetrical 210 mM K^+ in the presence of 10 mM Ca^{2+} in both *cis* and *trans* chambers (see below). The magnitude of the asymmetry of block was small at these holding potentials for both Ba^{2+} and Ca^{2+} (see Fig. 7); the current in symmetrical 210 mM K^+ in the presence of 10 mM symmetrical Ba^{2+} was 17.9 ± 0.62 pA at $+60$ mV and -16.6 ± 0.67 pA at -60 mV ($n = 5$, ±SEM). The reduced current is expressed as a proportion of the control current and the final ratio is the mean of the values at both positive and negative holding potentials. The pooled results of such experiments ($n = 5$) are shown in Fig. 6. In this figure the experimental points are shown together with curves derived from a computer simulation of the experiment using three different models for Ba^{2+}, in which the conductance is kept
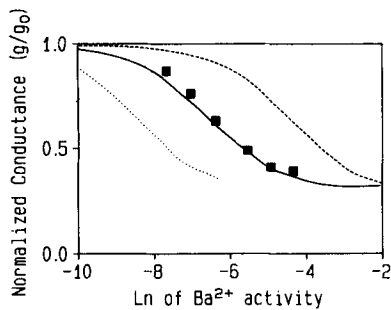

FIGURE 6. The reduction in single-channel current amplitude on the addition of a range of concentrations of Ba^{2+} expressed as a ratio of the control value in symmetrical 210 mM K^+ at a holding potential of ±60 mV. The data points are indicated by the filled squares ($n = 5$, ±SEM) and were a mean of the normalized conductances obtained at 60 and -60 mV. The solid line shows the model prediction with the energy profile for K^+ as detailed in Table I and for Ba^{2+} as in Table II. The dashed line was obtained with an energy profile for Ba^{2+} of peaks 1–4 = 5.5, wells 1 and 3 = -2.35, and the central well = -6.95 (in units of RT). The dotted line was obtained with an energy profile for Ba^{2+} of peaks 1–4 = 1.5, wells 1 and 3 = -2.35, and the central well = -11.0 (in units of RT). The energy profile for K^+ was the same in all three situations and is given in Table I. The best fit model has K_{D50} = 170 μM and E_{rev} = 36 mV (210 mM K^+ in the *cis* chamber and 210 mM Ba^{2+} in the *trans* chamber). The dashed line shows a model with K_{D50} = 2.25 mM and E_{rev} = 4 mV (210 mM K^+ in the *cis* chamber and 210 mM Ba^{2+} in the *trans* chamber), and the dotted line shows a model with K_{D50} = 30 μM and E_{rev} = 59 mV (210 mM K^+ in the *cis* chamber and 210 mM Ba^{2+} in the *trans* chamber). All three models for Ba^{2+} have a similar current amplitude at ±60 mV under saturating ionic conditions.

constant while peak height and well depth are varied to give different affinities for Ba^{2+} and different relative permeabilities for Ba^{2+}/K^+. The results correlate well with the model in which a K_D for Ba^{2+} of 170 μM and a reversal potential under bi-ionic conditions (Ba^{2+} *trans*, K^+ *cis*) of 36 mV are used. Details of the parameters used in the three models are given in the legend.

The second series of experiments examined the effect of Ca^{2+} added symmetrically or asymmetrically to the *trans* chamber and Mg^{2+} added only to the *trans* chamber. The reduction in single-channel conductance occurred over a range of concentrations similar to that seen with Ba^{2+}. The effects of 5 and 10 mM Ca^{2+} and Mg^{2+} were examined. In Fig. 7 *A* the experimentally observed single-channel current amplitudes obtained in symmetrical 210 mM K^+ with 5 mM Ca^{2+} added to the *trans* chamber are compared with the model prediction. In Fig. 7 *B* the current–voltage relationship
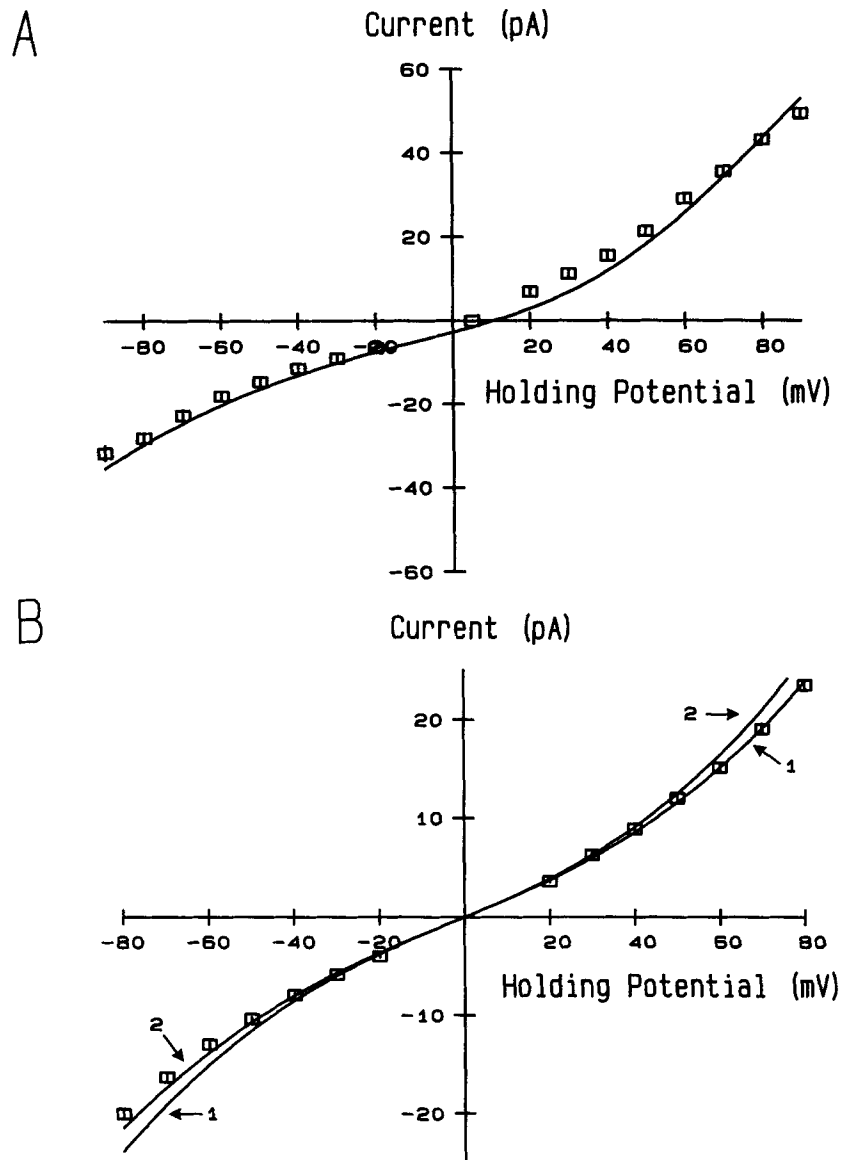
FIGURE 7.   (A) The single-channel current–voltage relationship in symmetrical 210 mM K^+ in the presence of 5 mM *trans* Ca^{2+}. The experimental points are indicated by squares (n = 4, ±SEM) and the line is the model prediction with the energy profiles for K^+ and Ca^{2+} as detailed in Tables I and II. (B) The single-channel current–voltage relationship in symmetrical 210 mM K^+ in the presence of 10 mM Ca^{2+} in both *cis* and *trans* chambers. The experimental points are indicated by squares (n = 5, ±SEM). The line marked 1 is the model prediction with the energy profiles for K^+ and Ca^{2+} as detailed in Tables I and II. The line marked 2 is a model prediction with a slightly shifted central binding site (0.03 toward the cytosolic face of the protein) but with otherwise identical energy profiles for K^+ and Ca^{2+} as detailed in Tables I and II.

obtained in symmetrical 210 mM K^+ in the presence of symmetrical 10 mM Ca^{2+} is compared with that predicted by the model (marked as line 1 in the figure). The simple model detailed in Tables I and II is able to give a reasonable fit to the data.

As noted above for Ba^{2+}, the experimentally determined current–voltage relationship in 210 mM K^+ with 10 mM Ca^{2+} added to both chambers is slightly asymmetric, with block being more apparent at negative holding potentials. This effect can be mimicked and the fit improved if the central binding site is shifted slightly toward the cytoplasmic face of the protein (line 2 of Fig. 7 B). The effect of this displacement of the central binding site on the symmetry of the current–voltage relationships modeled with symmetrical cations is small. For example, with a shift in the central
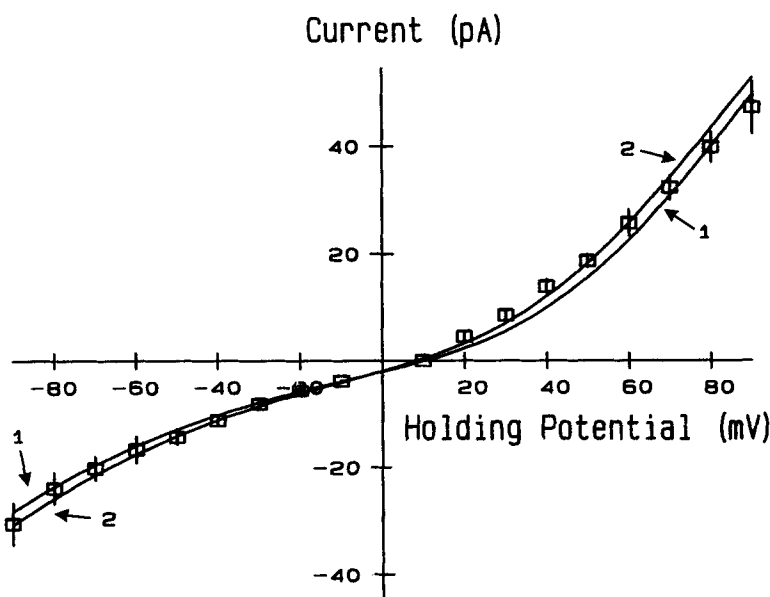

FIGURE 8. The single-channel current–voltage relationship in symmetrical 210 mM K^+ in the presence of 5 mM Mg^{2+} in the *trans* chamber. The experimental points are indicated by squares ($n = 5$, ±SEM). The line marked 1 is the model prediction using energy profile Mg^{2+}.1 and the line marked 2 is the model prediction using energy profile Mg^{2+}.2. The energy profiles are both given in Table II.

binding site as detailed in the legend to Fig. 7, the predicted single-channel current amplitudes at 80 and −80 mV holding potential in symmetrical 210 mM K^+ are 58.51 and −56.53 pA, respectively.

The addition of 5 mM Mg^{2+} or Ca^{2+} to the *trans* chamber leads to only a small change in the reversal potential (generally 5–10 mV) and this is compatible with the previously determined relative permeabilities of these ions to K^+.

The symmetry inherent in the voltage- and concentration-independent energy profiles of K^+ and the alkaline earth divalent cations and the assumption of the peak offset condition between the ions imply that the zero-current potential is the same whether the divalent solution is bathing the cytosolic or the luminal face of the

protein. This model prediction is borne out experimentally for Ba^{2+} and Sr^{2+} (see Tinker and Williams, 1992).

Explaining the Differences in Divalent Cation Conductance

The divalent cations display significant differences in conductance but only small differences in permeability. This is analogous to the situation found with the monovalent cations. In the latter case the model explains this by differing affinities of a central binding site for the conducting ion, and this proposition is given support by the similarity between the predicted and observed values of K_D and G_{max} as determined from the conductance–activity relationships (Table III). Two possibilities
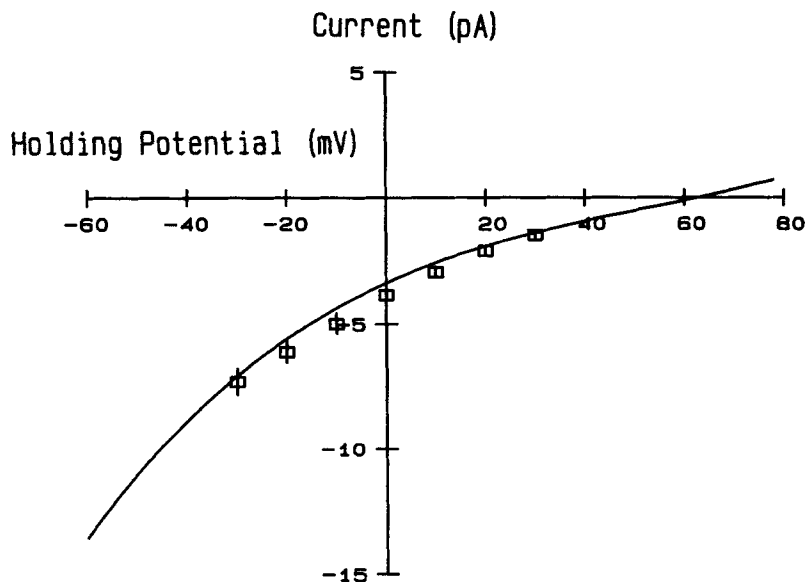

FIGURE 9. The single-channel current–voltage relationship obtained after the fusion of a native SR membrane vesicle. The *trans* chamber contains 60 mM free Ca^{2+} and the *cis* chamber contains 125 mM $Tris^+$. The experimental points are indicated by the squares (n = 9, ±SD; data taken from Williams and Holmberg, 1990). The smooth line is the fit generated by the model given in Tables I and II.

exist to explain the difference in conductance seen, for example, between Ca^{2+} and Mg^{2+} in this simple model. The first is that peak height and thus permeability are similar and the lower conductance of Mg^{2+} is accounted for by higher central site affinity. The second is that the affinity of the conduction pathway for the two ions is similar but Mg^{2+} has higher peak heights and thus a lower permeability than Ca^{2+}, relative to K^+, resulting in a lower conductance. Unfortunately, as described in the preceding paper (Tinker and Williams, 1992), it is not possible to approach the K_D for Ba^{2+}, near-maximal conductance being observed at an activity of 1.7 mM. By extension, it seems probable that this will also be the case for the other divalents. Is it possible to use the concentration dependence of divalent block of monovalent
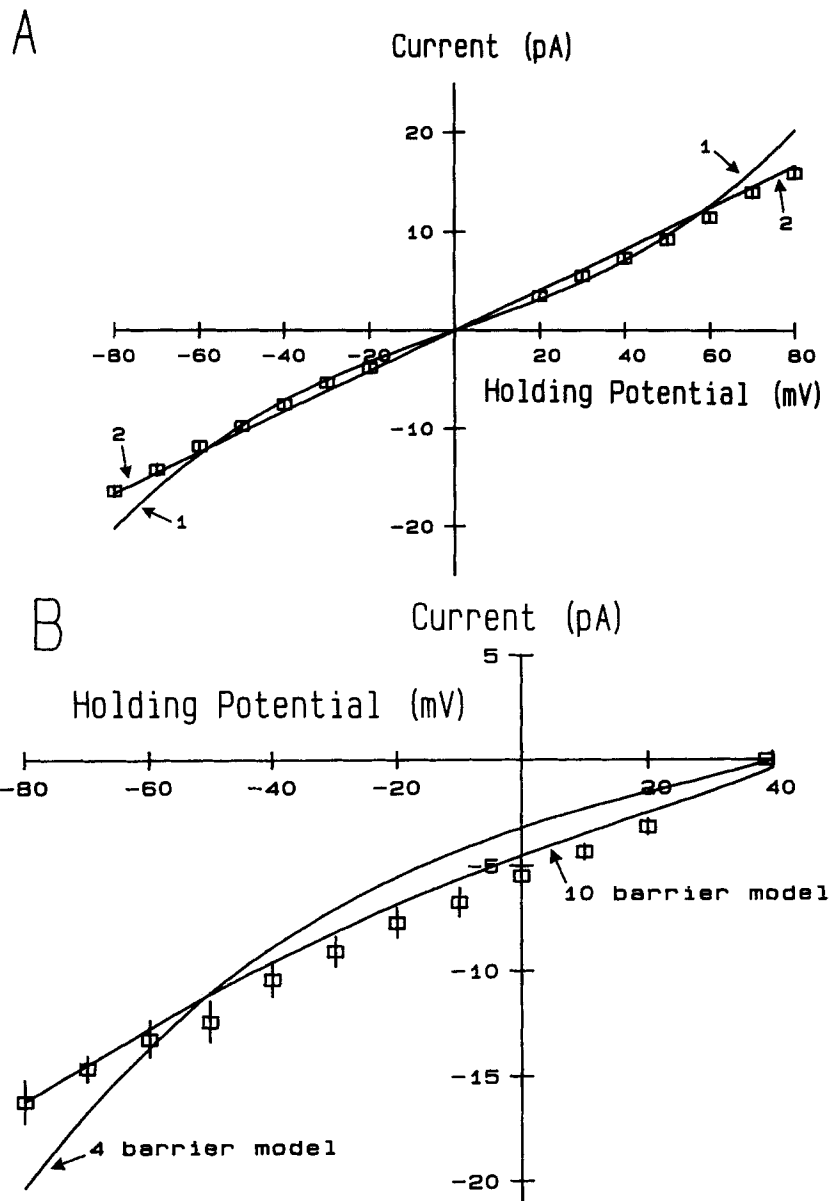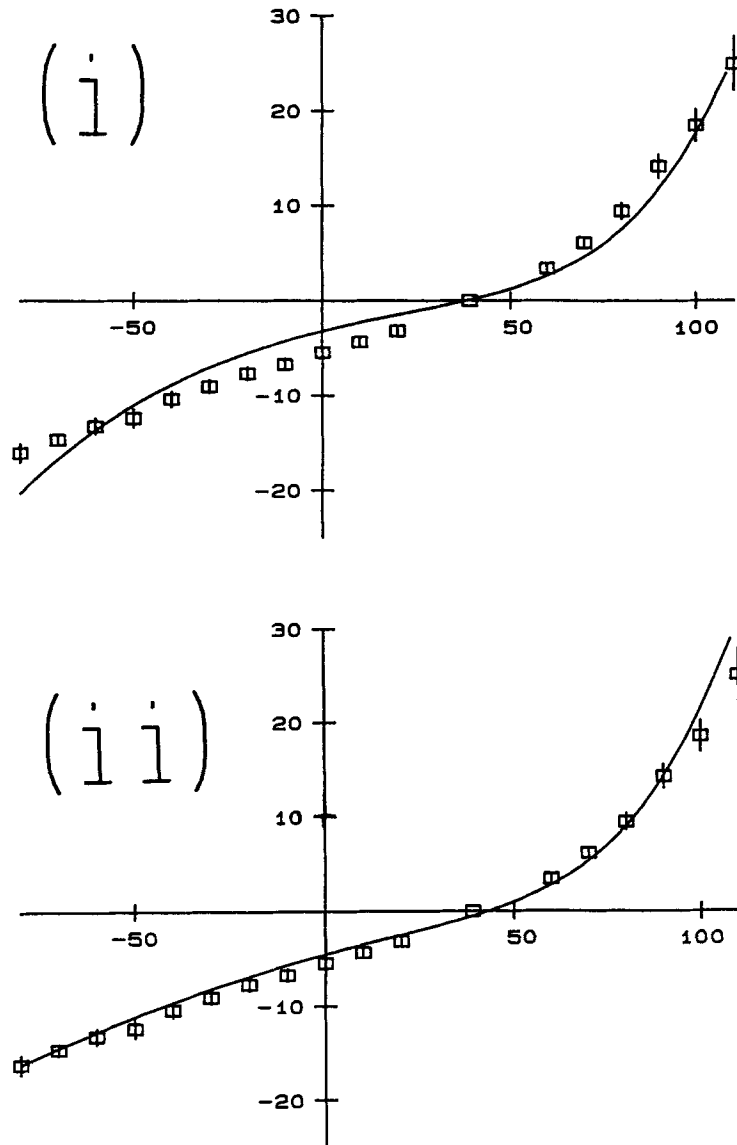
FIGURE 10. (A) The fits generated by the 4-barrier model for Ba^{2+} given in Table II (line marked 1 on diagram) and a 10-barrier model for Ba^{2+} (peaks 1–10 = 2.38, wells 1–4 and wells 6–9 = -0.8, and the central well = -8.8, in units of RT; line marked 2 on the diagram) are shown together on the figure for comparison. The conduction parameters generated by the 10-barrier model are similar to those of the 4-barrier model; K_{D50} = 150 μM and $P_{Ba^{2+}}/P_{K^+}$ = 5.28 under bi-ionic conditions with 210 mM salt. The experimental points are indicated by squares and are from the previous paper (n = 5, ±SEM). The curve generated by the 10-barrier model is more ohmic and fits the data better at high positive and negative voltages. (B) The single-channel current–voltage relationship under bi-ionic conditions with 210 mM K^+ in the *cis* chamber and 210 mM Ca^{2+} in the *trans* chamber. The data points are from Tinker

and Williams (1992) and are indicated by squares (n = 5, ±SEM). The remaining two panels in the figure show the fit generated to the points from the 4-barrier model (i) and the 10-barrier model (ii) over the complete voltage range. The curves generated by the 4- and 10-barrier models are compared over a more limited voltage range in the rest of the figure. The points negative to the reversal potential represent increasingly pure Ca^{2+} current as the holding potential becomes more negative. Unlike the 4-barrier model, the 10-barrier model, is able to reproduce the largely ohmic behavior in this region. The 4-barrier fit was generated by the energy profiles given in Tables I and II. The energy profiles for the 10-barrier model are for Ca^{2+} peaks 1–10 = 2.00, wells 1–4 and wells 6–9 = −0.8, and the central well = −9.25, and for K^+ peaks 1–10 = 4.63, wells 1–4 and wells 6–9 = −0.8, and central well = −3.25 (in units of RT). The conduction parameters generated by the 10-barrier model are similar to those of the 4-barrier model; K_{D50} = 100 vs. 110 µM and E_{rev} = 43.1 vs. 39.9 mV.

current to answer this question? Fig. 8 shows the comparison of two models, one where central binding accounts for the difference in conductance seen between Ca^{2+} and Mg^{2+} (using profile $Mg^{2+}.1$ of Table II) and the other where there is a small difference in permeability but no difference in central site affinity between the two ions (using profile $Mg^{2+}.2$ of Table II). It can be seen that both models give reasonable fits to the data and, if anything, the fit generated by the energy profile $Mg^{2+}.2$ (Table II and line 2 in Fig. 8) is closer. The model then suggests that such experiments are not sufficiently sensitive to pick up the small changes in affinity that may be responsible for the differences seen in conductance. The fits generated on the basis of energy profile $Mg^{2+}.1$ are compatible with the data but do not exclude other possibilities.

Modeling Conduction in the Ryanodine Receptor Channel from Native SR Membranes

The presence of Cl^- and K^+ channels in SR membrane vesicles limits the ionic composition of solutions under which pure current through the ryanodine receptor channel can be examined after the incorporation of native SR vesicles into planar bilayers. The properties of native ryanodine receptor channels are conventionally examined with high concentrations of Ca^{2+} at the luminal face and $Tris^+$ at the cytosolic face of the channel (Smith, Coronado, and Meissner, 1985; Ashley and Williams, 1990). The ability to model conduction of these ions allows us to subject our approach to a completely independent test. Fig. 9 shows the predicted single-channel current–voltage relationship compared with experimental points determined for the Ca^{2+} release channel from native SR membrane vesicles with 60 mM Ca^{2+} in the *trans* and 125 mM $Tris^+$ in the *cis* solution. The fit is reassuringly close and lends further support to the proposal that our method of channel purification does not significantly modify the conduction pathway. The shape of the current–voltage relationship suggests that performing linear regression on the individual current points and extrapolating the line as has been routinely done to estimate the reversal potential may underestimate the $Ca^{2+}/Tris^+$ permeability ratio. The current reverses at 62 mV in the model, yielding a $Ca^{2+}/Tris^+$ permeability ratio of 78. In addition, the presence of *cis* $Tris^+$ reduces the true single-channel conductance. Even at 0 mV holding potential, 2% of the channels will be occupied by $Tris^+$ (or alternatively, the probability of a single open channel being occupied by $Tris^+$ is 0.02) under these ionic conditions.

Some Weaknesses of This Simple Model

The current–voltage relationships predicted by the model for the divalent cations are not as linear as those found experimentally. The effect is especially prominent at high holding potentials and is illustrated under symmetrical and bi-ionic conditions in Fig. 10, A and B. Inconsistencies of this kind have been commented on, in a general sense, by Levitt (1986) and constitute one of the arguments he uses to support the use of the Nernst-Planck continuum theory as opposed to the reaction rate theory. It is highly unlikely that ion translocation through the ryanodine receptor channel occurs as four discrete steps, and the fit to the data for the divalent cation current–voltage relationships can be improved by increasing the number of

barriers. Fig. 10, *A* and *B*, shows the comparison of the 4-barrier models given in Tables I and II, with 10-barrier models producing similar conduction properties (see legend to Fig. 10). A major difference is that the 10-barrier models have considerably more linear current–voltage relationships with divalent cations as the permeant species, and as a result these relationships do not deviate from the experimental points at high negative and positive holding potentials. Such models begin to approximate a continuum solution, but they do introduce a large number of free variables without materially altering the general conclusions derived from much simpler schemes. We thus retain the simpler model while appreciating this limitation.

The conductance for Mg^{2+} predicted by the model (Table IV) is higher than obtained experimentally under bi-ionic conditions (see Tinker and Williams, 1992). This discrepancy is larger in percentage terms than for the other ions studied. It is possible to approach the experimental figure by combining higher peak height and higher central site affinity relative to Ca^{2+}. For example, if peaks 1–4 = 3.3, wells 1 and 3 = −2.35, and central well = −9.8 (units of RT) the modeled conductance in 210 mM salt between −60 and +60 mV holding potential is 95 pS. This improvement occurs at the expense of the fit to Mg^{2+} block of K^+ current. In the ensuing discussion the $Mg^{2+}.1$ energy profile is adopted as a reasonable, though by no means perfect, approximation to the behavior of Mg^{2+}.

DISCUSSION

Mechanisms of Ion Translocation and Discrimination

In general, there is close agreement between the model predictions for ion translocation and discrimination in the ryanodine receptor channel and the experimental data, even under quite complicated mixed ionic conditions with both monovalent and divalent cations. As a consequence of this close correlation, in the following discussion we will assume that the model provides a valid, albeit simplified, working description of ion translocation and discrimination in the receptor channel. The central ion binding site of the model is taken to be equivalent to the TMA^+ blocking site identified in previous studies from this laboratory (Tinker et al., 1992).

The findings of this study strongly support predominantly single-ion occupancy for the ryanodine receptor channel under the described conditions. One of the strongest pieces of evidence indicating multi-ion occupancy in the L-type Ca^{2+} channel is the existence of at least two binding affinities. A K_D in the low micromolar range is necessary to explain the block of monovalent cation conduction by Ca^{2+} and another in the millimolar range is required to explain the conductance–activity relationship obtained for Ca^{2+} (Tsien, Hess, McCleskey, and Rosenberg, 1987). In the ryanodine receptor channel the estimates of divalent K_D obtained from block of monovalent flux and those derived from conductance saturation are much closer and are compatible with a single binding affinity. In addition, the modeling process gives us insights into how ion discrimination might occur in the receptor channel.

Two broad processes govern ion translocation in the model. The peak height over each barrier is less for divalent cations than monovalent cations. This process also leads to a weak discrimination between Cs^+ and the other monovalents and similarly

between Ba^{2+} and the other divalents. The overall order of peak heights is Cs^+ > $Na^+ = K^+ = Li^+ \gg Ba^{2+} > Mg^{2+} = Ca^{2+} = Sr^{2+}$.

The second important factor is the existence of a central binding site. This site shows a much higher affinity for divalent as opposed to monovalent cations. Furthermore, it shows discrimination between the individual monovalent cations, binding, in order of increasing affinity, $Cs^+ < K^+ < Na^+ < Li^+$. Similarly, the central binding site discriminates between the individual divalent cations with an order of increasing affinity $Ba^{2+} < Sr^{2+} < Ca^{2+} < Mg^{2+}$. Implicit in the model is the assertion that the differences in conductance among the individual monovalents and among the individual divalents are largely accounted for by differing affinity at this site. The difference between monovalents and divalents as broad groups results from the specificity of this site and a thermodynamic process that favors the passage of divalent as opposed to monovalent cations between binding sites through the ryanodine receptor channel. These two factors make the ryanodine receptor channel a "calcium channel," or perhaps more correctly, a divalent cation channel. The different energy profiles for Ca^{2+} and K^+ are illustrated in Fig. 11.
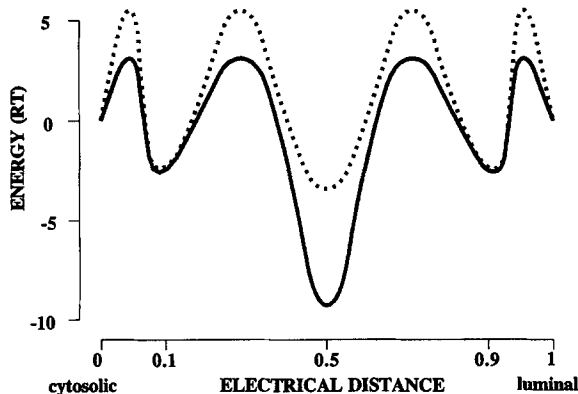

FIGURE 11. Comparison of the voltage- and concentration-independent energy profiles for K^+ (dotted line) and Ca^{2+} (solid line) given in Tables I and II, respectively.

One of the paradoxes of selectivity achieved by high affinity binding is that conductance decreases as affinity increases. The ryanodine receptor channel, acting as a single-ion pore, ameliorates this by favoring the passage of divalent as opposed to monovalent cations between binding sites. Another solution, proposed for the L-type Ca^{2+} channel, is that ion to ion interactions in multiply occupied states within a multi-ion pore enhance the exit of Ca^{2+} from the channel and thus increase the conductance. The latter effect allows a higher degree of selectivity to be achieved in this species of channel than is observed in the ryanodine receptor channel.

Possible Physical Structures Responsible for Selectivity

The above arguments immediately lead to the question of the nature of the physical structures that might underlie the two processes governing selectivity. To some extent this very rigid distinction between the two processes is artificial, as the energies of peaks and wells are not very dissimilar. Energetic maxima represent only slightly less favorable energetic locations than minima.

The sequence for monovalent cation binding to the central site corresponds to an Eisenman sequence XI, and for the divalent cations the sequence corresponds to sequence VII as determined by Sherry (1969). The common factor linking these two sequences is that they are the sequences predicted for a high field strength site (Diamond and Wright, 1969; Eisenman and Horn, 1983). At such sites the energetic balance between the ion-site interaction energy and the dehydration energy increasingly favors the binding of ions as the crystal radii decrease. Such a site, in general, binds divalent cations with a much higher affinity than monovalents. We have proposed the existence of two sites within the conduction pathway of the receptor channel to which the small tetraalkyl ammonium cations bind (Tinker et al., 1992). The central site, which we take to be the central cation binding site of the model, binds TMA^+ but not the larger members of the group.

From these observations is it possible to speculate on the possible structure of the site? The proposed affinity of the site lies much more in the range of the extracellular enzymes and proteins that bind Ca^{2+}, such as bovine β-trypsin, than in the intracellular EF hand group of proteins (Strynadka and James, 1989). In general, Ca^{2+} binds in both groups of proteins in a multiple liganded structure with either six, or more commonly seven, coordinated oxygen ligands (Strynadka and James, 1989). The oxygens involved could be provided, for example, by high field strength carboxyl groups. Mg^{2+} (a smaller ion than Ca^{2+}) binding would be favored over Ca^{2+} if the liganding groups approached the binding ion more closely (Strynadka and James, 1989). TMA^+ is approximately the size of Ca^{2+} with a single water of hydration and it is intriguing that many of the calcium binding proteins bind Ca^{2+} in such a state (Heizmann and Hunziker, 1991).

What kind of physical structure will favor the passage between binding sites of divalent rather than monovalent cations, or, to use a chemical analogy, reduce the activation energy for divalents? One clue comes from studies of the specificity of hydrated alkali-aluminium silicates (zeolites), in some of which, contrary to theoretical expectation, monovalent cations were preferred to divalents (Sherry, 1969). The critical factor governing discrimination was found to be the site density: those with closely spaced sites preferred divalents, while those with widely spaced sites selected monovalents. Models of glass electrodes with high specificity for divalent cations also suggest that intersite spacing is of critical importance (Truesdell and Christ, 1967). A similar situation may pertain in the conduction pathway of the sheep cardiac SR ryanodine receptor channel: the site charge density may be high and so give high divalent permeability. The charge could be located in the narrow part of the pore but might also be within vestibules to either side of this region (Dani, 1986).

Problems of Selectivity and Conductance

A major theoretical problem posed by the observed and modeled conductance properties of the ryanodine receptor channel is the combination of high conductance with significant selectivity. Most channels displaying any degree of discrimination have a much smaller conductance than the ryanodine receptor channel. The magnitude of the problem can be appreciated by estimating the rate of entry of ions into the pore in the absence of a driving potential. If the on rate constant (K_{on}) is diffusion limited and the channel is a circular receptor of radius r, then (Almers and

McCleskey, 1984; Hille, 1984):

$$K_{on} = 2 \cdot \pi \cdot r \cdot D \cdot N \cdot 10^{-3}$$

where D is the diffusion coefficient for the ion and N is Avogadro's number. We can estimate r as the radius of the largest permeable ion, $Tris^+$ (~0.36 nm), and D for K^+ and Ca^{2+} is 19.6 E-6 and 8 E-6 cm^2/s, respectively (Hille, 1984). Thus K_{on} can be calculated as 1.09 E9 s^{-1} and 2.67 E9 s^{-1} for Ca^{2+} and K^+, respectively, which corresponds to barriers of 8.7 and 7.8 for these ions at 20°C. These figures correspond to the first barrier for ion entry and are much higher than the figures we have used in the model (see Fig. 11). Even if ion entry and exit are assumed to be essentially rate limiting, the discrepancy between the best fit models and the values of K_{on} determined from diffusion limitation is still large. What are the possible solutions to this paradox?

One solution would be if the pore radius of the receptor channel was considerably greater than the value estimated from $Tris^+$. However, it is difficult to envisage a pore with the necessary radius maintaining any degree of contact with, and hence, discrimination between, translocating ions.

Another possibility is that the effective radius of the pore with which ions collide before entering the voltage drop is much larger than the narrowest part of the conduction pathway estimated from $Tris^+$ conduction. The arrangement of wide channel mouths on either side of a short constriction at which ion selectivity occurs has been suggested as a structural arrangement by which some channels achieve both high conductance and selectivity (Latorre and Miller, 1983).

High conductance, with the retention of the degree of selectivity displayed in the ryanodine receptor channel, might also be achieved if the functional receptor channel is composed of a number of identical conduction pathways that gate in a coordinated fashion to produce the observed unit conductance. Evidence in support of this possibility comes from the appearance of distinct subconductance states in the recordings of purified ryanodine receptor channels produced by other groups (Ma, Fill, Knudson, Campbell, and Coronado, 1988; Liu, Lai, Rousseau, Jones, and Meissner, 1989) and the observation of multiple "channels" in ultrastructural studies of receptor channels (Wagenknecht, Grassucci, Frank, Saito, Inui, and Fleischer, 1989). In practice, it is likely that a combination of these factors enables the receptor channel to achieve such high single-channel conductance.

What then is the overall physical view for ionic conduction in this channel? The ryanodine receptor channel may well consist of a number of identical single-ion conduction pathways arranged in parallel. Each of these pathways has a wide mouth or vestibule at either side of a short constriction. Ions are influenced by voltage in the mouth regions and swept toward the short constriction, entering this region without any significant dehydration. The ions are dehydrated on entry into a high field strength divalent cation binding site and are subsequently rehydrated on leaving this site. The location in the voltage drop across the receptor channel at which tetraethyl ammonium and tetrapropyl ammonium interact to block K^+ conductance indicates that the point of maximal pore narrowing probably occurs close to the luminal face of the protein (Tinker et al., 1992). Ions probably remain relatively hydrated on passage

through this region. Both the mouths and narrow regions of the pore are lined with a relatively high density of negative charge.

Conduction Properties of the Ryanodine Receptor Channel in Mixtures of Permeant Ions

Our model of ionic conduction in the sheep cardiac muscle ryanodine receptor channel enables us to make some predictions concerning the nature of the current carried in the channel in the presence of ionic conditions approaching those found in the cardiac cell. It has previously been suggested that the relatively high conductance of K^+ in the ryanodine receptor channel might produce a situation where both K^+ and Ca^{2+} counter-currents flow simultaneously, with K^+ current providing charge compensation during Ca^{2+} flux across the SR membrane (Smith, Coronado, and Meissner, 1986). With 120 mM symmetrical K^+, a cytosolic free Ca^{2+} in the low micromolar range, and an approximate intraluminal free Ca^{2+} of 2.5 mM (Ikemoto, Antoniu, Kang, Meszaros, and Ronjat, 1991; Wendt-Gallitelli and Isenberg, 1991), at 0 mV the model predicts a single-channel current of close to 3 pA and a reversal potential of 11 mV. 76% of the channels are carrying Ca^{2+} current, 5% are unoccupied, and 19% are occupied by K^+ (this alternatively represents the probability of a single channel being occupied by a particular ion). Therefore, the selectivity that the receptor channel does show guarantees that under physiological conditions a very large proportion of channels will be carrying Ca^{2+} current and will be unable to act as their own charge compensators during Ca^{2+} release from the SR. This role will be carried out by the SR K^+ and Cl^- channels. A more complete analysis of ion flux through the ryanodine receptor channel under physiological conditions will be possible when Mg^{2+} is included in the model.

The high divalent conductance described is ideally suited to the mass transport of Ca^{2+} from the SR into the cytoplasm. In addition, the low K_m for the divalents will enable maximal conductance to be achieved at concentrations of 2–3 mM, the probable Ca^{2+} concentration in the SR (Ikemoto et al., 1991; Wendt-Gallitelli and Isenberg, 1991).

Further Possibilities for Modeling

There is a danger of becoming beguiled by the mathematical predictions of rate theory models and over-interpreting energy profiles. It is very tempting to equate energetic barriers with actual physical structures. In a general sense this is possible, for example, when comparing divalent with monovalent cations as above. It has been argued (Levitt, 1986, 1991) that an approach based on the Nernst-Planck continuum theory may be more physically realistic. Such a model has its attractions for the sheep cardiac SR ryanodine receptor channel. The possible existence of large vestibules is likely to mean that the energy profile varies relatively smoothly in these regions and ion transport is probably best described here by an electrodiffusion approach. In addition, continuum models will give more linear current–voltage relationships. Unfortunately, our current state of structural knowledge is inadequate to attempt such an approach. Until such information becomes available the assumptions of the continuum theory will be as, if not more, arbitrary than the Eyring rate theory.

In summary, ionic conduction appears to be governed by relatively simple

processes in the ryanodine receptor channel. The quantitative predictions of the rate theory model support single-ion occupancy. The model suggests that discrimination between divalent and monovalent cations occurs because of a high affinity divalent binding site located centrally in the voltage drop and a process that favors the passage of divalents between binding sites. Furthermore, differences in conductance among the group Ia cations and among the alkaline earths are largely explained by differing affinity at this putative central site.

REFERENCES

Almers, W., and E. W. McCleskey. 1984. Non-selective conductance in calcium channels of frog muscle: calcium selectivity in a single-file pore. *Journal of Physiology.* 353:585–608.

Ashley, R. H., and A. J. Williams. 1990. Divalent cation activation and inhibition of single calcium release channels from sheep cardiac sarcoplasmic reticulum. *Journal of General Physiology.* 95:981–1005.

Dani, J. A. 1986. Ion-channel entrances influence permeation. Net charge, size, shape and binding considerations. *Biophysical Journal.* 49:607–618.

Diamond, J. M., and E. Wright. 1969. Biological membranes: the physical basis of ion and nonelectrolyte selectivity. *Annual Review of Physiology.* 31:581–646.

Eisenman, G., and R. Horn. 1983. Ionic selectivity revisited: the role of kinetic and equilibrium processes in ion permeation through channels. *Journal of Membrane Biology.* 76:197–225.

Goldman, D. E. 1943. Potential, impedance, and rectification in membranes. *Journal of General Physiology.* 27:37–60.

Heizmann, C. W., and W. Hunziker. 1991. Intracellular calcium-binding proteins: more sites than insights. *Trends in Biochemical Sciences.* 16:98–103.

Hille, B. 1975. Ionic selectivity, saturation and block in sodium channels. A four barrier model. *Journal of General Physiology.* 66:535–560.

Hille, B. 1984. Ionic Channels of Excitable Membranes. Sinauer Associates, Inc., Sunderland, MA. 249–271.

Hodgkin, A. L., and B. Katz. 1949. The effect of sodium ions on the electrical activity of the giant axon of the squid. *Journal of Physiology.* 108:37–77.

Ikemoto, N., B. Antoniu, J.-J. Kang, L. G. Meszaros, and M. Ronjat. 1991. Intravesicular calcium transient during calcium release from sarcoplasmic reticulum. *Biochemistry.* 30:5230–5237.

King, E. L., and C. Altman. 1956. A schematic method of deriving the rate laws for enzyme-catalysed reactions. *Journal of Physical Chemistry.* 60:1375–1378.

Kortum, G., and J. O'M. Bockris. 1951. Textbook of Electrochemistry. Elsevier Science Publishers B.V., Amsterdam. 680–681.

Latorre, R., and C. Miller. 1983. Conduction and selectivity in potassium channels. *Journal of Membrane Biology.* 71:11–30.

Lauger, P. 1973. Ion transport through pores: a rate-theory analysis. *Biochimica et Biophysica Acta.* 311:423–441.

Lauger, P., W. Stephan, and E. Frehland. 1980. Fluctuations of barrier structure in ionic channels. *Biochimica et Biophysica Acta.* 602:167–180.

Levitt, D.G. 1986. Interpretation of biological ion channel flux data: reaction-rate versus continuum theory. *Annual Review of Biophysics and Biophysical Chemistry.* 15:29–57.

Levitt, D. G. 1991. General continuum theory for multiion channel. I. Theory. *Biophysical Journal.* 59:271–277.

Lindsay, A. R. G., S. D. Manning, and A. J. Williams. 1991. Monovalent cation conductance in the ryanodine receptor-channel of sheep cardiac muscle sarcoplasmic reticulum. *Journal of Physiology.* 439:463–480.

Liu, Q.-Y., F. A. Lai, E. Rousseau, R. V. Jones, and G. Meissner. 1989. Multiple conductance states of the purified calcium release channel complex from skeletal sarcoplasmic reticulum. *Biophysical Journal.* 55:415–424.

Lobo, V. M. M. 1989. Handbook of Electrolyte Solutions. Elsevier Science Publishers B.V., Amsterdam.

Ma, J. J., M. Fill, M. Knudson, K. P. Campbell, and R. Coronado. 1988. Ryanodine receptor of skeletal muscle is a gap junction-type channel. *Science.* 242:99–102.

Sherry, H. S. 1969. The ion-exchange properties of zeolites. *In* Ion Exchange. J. Marinsky, editor. Marcel Dekker, Inc., New York. 89–133.

Smith, J. S., R. Coronado, and G. Meissner. 1985. Sarcoplasmic reticulum contains adenine nucleotide-activated calcium channels. *Nature.* 316:446–449.

Smith, J. S., R. Coronado, and G. Meissner. 1986. Single channel measurements of the calcium release channel from skeletal muscle sarcoplasmic reticulum. *Journal of General Physiology.* 88:573–588.

Strynadka, N. C. J., and M. N. G. James. 1989. Crystal structures of the helix-loop-helix calcium-binding proteins. *Annual Reviews of Biochemistry.* 58:951–998.

Tinker, A., A. R. G. Lindsay, and A. J. Williams. 1992. Block of the sheep cardiac sarcoplasmic reticulum Ca^{2+}-release channel by tetra-alkyl ammonium cations. *Journal of Membrane Biology.* 127:149–159.

Tinker, A., and A. J. Williams. 1992. Divalent cation conduction in the ryanodine receptor channel of sheep cardiac muscle sarcoplasmic reticulum. *Journal of General Physiology.* 100:479–493.

Truesdell, A. H., and C. L. Christ. 1967. Glass electrodes for calcium and other divalent cations. *In* Glass Electrodes for Hydrogen and Other Cations. G. Eisenman, editor. Marcel Dekker, Inc., New York. 293–321.

Tsien, R. W., P. Hess, E. W. McCleskey, and R. L. Rosenberg. 1987. Calcium channels: mechanisms of selectivity, permeation and block. *Annual Review of Biophysics and Biophysical Chemistry.* 16:265–290.

Wagenknecht, T., R. Grassucci, J. Frank, A. Saito, M. Inui, and S. Fleischer. 1989. Three-dimensional architecture of the calcium channel/foot structure of sarcoplasmic reticulum. *Nature.* 338:167–170.

Wendt-Gallitelli, M. F., and G. Isenberg. 1991. Total and free myoplasmic calcium during a contraction cycle: X-ray microanalysis in guinea-pig ventricular myocytes. *Journal of Physiology.* 435:349–372.

Williams, A. J., and S. R. M. Holmberg. 1990. Sulmazole (AR-L 115BS) activates the sheep cardiac muscle sarcoplasmic reticulum calcium-release channel in the presence and absence of calcium. *Journal of Membrane Biology.* 115:167–178.